American Mineralogist, Volume 82, pages 1079–1090, 1997

Analytical electron microscopy of nanometer-scale hornblende lamellae: Low-temperature exsolution in cummingtonite

Ulrich Klein,[1,*] Thomas G. Sharp,[2,†] and John C. Schumacher[1]

[1]Institut für Mineralogie, Petrologie und Geochemie der Albert-Ludwigs-Universität zu Freiburg, Albertstrasse 23b, 79104 Freiburg i. Br., Germany
[2]Bayrisches Geoinstitut, Universität Bayreuth, 95440 Bayreuth, Germany

Abstract

Cummingtonite from central Massachusetts, which has experienced pervasive exsolution of hornblende, contains numerous hornblende precipitates (lamellae and discs) ranging in thickness from 2.5 μm to 4 nm that represent multiple generations of exsolution. The smallest precipitates were investigated using transmission electron microscopy and analytical electron microscopy to characterize the coherent cummingtonite-hornblende solvus at low temperature. In contrast to older (coarser) generations of exsolution lamellae, which are 0.5–2.5 μm in width, planar, and extend across entire grains, the youngest generation consists of nanometer-scale discs (4–80 nm thick and 10–1000 nm long) that represent exsolution at approximately 300 °C (Klein et al. 1996). Quantitative energy-dispersive X-ray analyses were obtained from discs as small as 20 nm in thickness, providing compositional data for coherent exsolution of hornblende at ~300 °C. Surprisingly, these tiny discs have a lower Ca content and a higher Al content than the coarser, higher temperature lamellae. These compositions appear to lie well within miscibility gaps of the equilibrium and coherent solvi for cummingtonite-hornblende (in terms of Ca ↔ Fe^{2+} exchange) at low temperatures, and may represent a more tschermakitic hornblende coexisting with cummingtonite with excess Al relative to Ca. The composition of the cummingtonite host between nanometer-scale discs is very low in both Ca and Al relative to bulk cummingtonite analyses that were obtained from electron microprobe analyses of 1–2 μm areas.

Compositional profiles across host areas were measured to help interpret the unexpected chemistries of the nanometer-scale discs. A profile across the precipitate-free zone between a coarse hornblende lamella and a group of nanometer-scale hornblende discs shows downward concavity for Ca and Al, as expected for incomplete diffusion between the precipitation zone and the pre-existing hornblende lamellae. A profile measured between two nanometer-scale discs shows downward concavity for Al and nearly constant to slight upward concavity for the Ca content, suggesting incomplete Al diffusion before completion of the exsolution process, but a near-equilibrium state for Ca. However, the Ca profile could also represent incomplete diffusion, if the hornblende discs had started coarsening at the expense of other (shrinking) discs by means of the Gibbs-Thomson (capillary) effect. The observed profiles suggest that, relative to Al, Ca was the faster diffusing element when the exsolution and coarsening processes stopped.

Introduction

Exsolution in mineral solid solutions has long been used for geothermometry to interpret thermal histories of igneous and metamorphic rocks (e.g., Ross et al. 1969; Robinson et al. 1977). The presence of multiple generations of exsolution lamellae allows the interpretation of complex thermal histories, if the means of determining exsolution temperatures for the various generations exists. Recent work by Klein et al. (1996) and Schumacher et al. (1993) has demonstrated the existence of multi-generational exsolution among Ca- and Fe,Mg-containing clinoamphiboles in amphibolites from New England on the basis of the sizes and orientations of the lamellae.

The exsolved cummingtonite that was used in this study is from an amphibolite of Middle Ordovician age from the Partridge Formation (Hollocher 1993) from central Massachusetts (also see Schumacher 1988). Peak Devonian metamorphic conditions that are estimated for the sample (Q-603C) were ~675 °C and ~6 kbar (Hollocher 1985). Hornblende precipitates range in thickness from 2.5 μm lamellae down to 4 nm discs. The nanometer-

* Present address: Mineralogisch-Petrographisches Institut der Christian-Albrechts-Universität zu Kiel, Olshausenstrasse 40, 24098 Kiel, Germany.
† Present address: Department of Geology, Arizona State University, Tempe, Arizona 85287-1404, U.S.A.

0003–004X/97/1112–1079$05.00

scale discs were first shown to be chemically distinct from the surrounding host and therefore exsolution products by using electron spectroscopic imaging with the Ca_{L_2,L_3} edge (Czank et al. 1993, 1997).

Analytical electron microscopy (AEM) studies of exsolved amphiboles [e.g., by Smelik and Veblen (1989, 1991, 1993) and Smelik et al. (1991)] demonstrated the importance of this method for obtaining mineral analyses from exsolution features that are much smaller than those routinely measured by electron microprobe analysis (EMA). Recent applications of AEM to the measurement of compositional zoning in minerals have shown that the high spatial resolution of the technique can be used to measure micrometer-scale to submicrometer-scale diffusion profiles in minerals to provide diffusion data (Meissner et al. 1996) as well as constraints on metamorphic histories (Ganguly et al. 1996). In this paper we apply analytical electron microscopy to nanometer-scale hornblende lamellae in cummingtonite to investigate the chemistry of late-stage and low-temperature exsolution.

In clinoamphiboles the two common orientations for exsolution lamella are parallel or nearly parallel to (100) and $(10\bar{1})$ (e.g., Vernon 1962; Jaffe et al. 1968; Ross et al. 1968, 1969; Robinson et al. 1969, 1971). These orientations correspond to the best coherent match between the structures and represent the optimal phase boundaries (OPB) (Bollman and Nissen 1968) and are designated as ''100'' and ''$10\bar{1}$''. The magnitude of the misfit between two coherently intergrown crystal lattices controls the crystallographic orientation of the lamellar-host interface such that the minimum strain energy occurs at an OPB orientation (Cahn 1968; Bollman and Nissen 1968; Robinson et al. 1971, 1977; Willaime and Brown 1974, 1985; Robin 1974, 1977; Fleet et al. 1980; Fleet 1982, 1984, 1985; Fleet and Arima 1985). Robinson et al. (1971, 1977) showed that the crystallographic orientation of exsolution lamellae in clinoamphiboles and clinopyroxenes can be calculated as a function of temperature by using the optimal phase boundary theory. Klein et al. (1996) used OPB theory and the orientations of lamellae in cummingtonite and hornblende samples from central Massachusetts to evaluate multi-generational exsolution. Klein et al. (1996) showed that the orientations of the different generations of exsolution lamellae do not vary as much as in the clinopyroxenes (Robinson et al. 1977), but the changes in orientation are measurable and can be used to estimate exsolution temperatures for individual amphibole samples. On the basis of OPB theory calculations it was possible to divide the $10\bar{1}$ oriented lamellae into different exsolution events, with respect to interface orientation and lamella thickness (Klein et al. 1996). The 100 lamellae orientations are predominantly controlled by the difference in c lattice parameters (Δc) between the hornblende and cummingtonite. Very small changes in Δc have tremendous effects on the 100 lamellae orientations. Consequently, 100 lamellae are too sensitive for the level of precision of the collected X-ray data to be useful exsolution temperature indicators. However, widths of both the 100 and $10\bar{1}$ lamellae cluster around a series of values, and, for the $10\bar{1}$ lamellae, decreasing lamellae widths can be correlated with lower exsolution temperatures.

In the transmission electron microscopy (TEM) investigations of cummingtonite (sample Q-603C) by Klein et al. (1996), widespread nanometer-scale precipitates of hornblende were found and interpreted as representing the last of at least six generations of exsolution. These precipitates are disc shaped and range in size from 4 to about 80 nm in width. In contrast to the older generations of lamellae, the nanometer-scale discs occur as large groups of homogeneously nucleated precipitates between the coarser, planar lamella systems with precipitate-free zones adjacent to the coarse lamella and increasing precipitate size with increasing distance from the larger lamellae. The small sizes of these hornblende discs and their textural relationships to the larger lamellae indicate that they represent the last stage of hornblende exsolution in the sample. Because of their lenticular shapes, it was not possible to determine the exact orientation of the precipitate-host boundaries, so that application of the OPB theory to the determination of the exsolution temperature is not as precise as with the coarse, planar lamellae. By using the angular relationships between of the major lattice vectors of the lamellae in the OPB theory, an exsolution temperature of approximately 300 °C was determined (Klein et al. 1996). Figure 1 shows a typical part of the sample with disc-shaped precipitates surrounded by coarse planar lamellae. A very interesting observation is that the orientation of the discs is generally not the same as the surrounding coarser lamellae (i.e., $10\bar{1}$ vs. 100 or 100 vs. $10\bar{1}$)

It is the purpose of the present study to show that these disk-shaped lamellae can be quantitatively analyzed using analytical electron microscopy. The compositions of these tiny lamellae and that of the pure host phase between them provide a detailed view of hornblende-cummingtonite exsolution processes at ~300 °C.

Cation exchanges between cummingtonite and Ca-rich hornblende

The hornblende composition is complex and is related to the chemistry of cummingtonite by several cation substitution mechanisms. There are three dominant substitution mechanisms relating cummingtonite to hornblende: (1) edenite substitution: $Na^{A} + {}^{[4]}Al \leftrightarrow \square^{A} + Si^{T}$, (2) tschermakite substitution: ${}^{[4]}Al + {}^{[6]}Al \leftrightarrow Mg^{M2} + Si^{T}$ and (3) M4 site: $Ca^{M4} \leftrightarrow Fe^{M4}$. Figure 2 shows a growing ''100'' hornblende lamella in cummingtonite host that is supersaturated with respect to Al, Na, and Ca. The growth of the lamella causes Al, Na, and Ca to diffuse through the host structure toward the lamella interface while Si, Fe, Mg, and A-site vacancies diffuse away from the growing lamella. If growth stops before the hornblende lamella equilibrates with all of the host cummingtonite, a ''stranded'' cation exchange profile should be present in the cummingtonite, which is concave upward for the elements diffusing away from the hornblende and con

FIGURE 1. A TEM image that shows the cummingtonite (Cum) host and two distinct hornblende (Hbld) lamellar systems. Note that all single-phase regions are well below the spatial resolution of EMA (about 1.5 μm). Image is taken in non-zone axis orientation.

cave downward for the cations diffusing toward the hornblende.

METHODOLOGY

Apparatus and experimental techniques

Our measurements were performed using a Philips CM20-FEG scanning transmission electron microscope equipped with a Super-twin objective lens and operated at 200 kV. This microscope is well suited for the analysis of nanometer-scale lamellae because it has a Schottky-type field-emission gun (FEG) that produces a very small, yet intense, electron beam. The beam current in an electron beam of 1 nm diameter (~0.5 nA) is high enough for quantitative energy-dispersive X-ray spectroscopy (EDS). The microscope is equipped with a germanium EDS detector and a Noran Voyager data acquisition and processing system.

All of our raw spectral data were quantified using experimentally determined Cliff-Lorimer k factors (Lorimer et al. 1972, 1973; Lorimer and Champness 1973; Cliff and Lorimer 1975) that were obtained using a hornblende standard (Arenai Volcano), which is part of the Smithsonian collection of natural mineral standards for EMA (Jarosewich 1975). The standard was measured 50 times using approximately the same microscope parameters as those used on the samples. Absorption was minimized by analyzing only sufficiently thin regions of the standard and sample. Because the k factors were obtained from approximately the same thickness of hornblende as our measurements, no absorption corrections were necessary. The sample thickness was held approximately constant by maintaining a constant X-ray count rate for a constant emission current from the field-emission gun. The averaged analyses of the standard were compared with the known chemistry to calculate Cliff-Lorimer k factors. These k factors, determined relative to Si, represent the detection efficiency for the various elements relative to Si. With the Cliff-Lorimer technique, the relative abundances of the elements are determined from the k factors and the ratio of X-ray intensities (see Peacor 1992). By specifying all of the elements present and their oxidation states, we can determine the concentration of oxides as well as a mineral formula.

The standard deviation of the mean of the X-ray intensities that were used to obtain the k factors determines the relative errors in the k-factors and therefore the element concentrations that are obtained from the k factors. Because we are most interested in errors that are introduced into the analyses, intensity values that were used in the standardization have been recast as element concentrations (weight percents), and their deviation from the average intensity shown as deviation from the concentrations in the standard (Fig. 3). Minor elements like Mn, Ti, and K in the hornblende standard have much larger relative errors than more abundant elements such as Si, Ca, and Mg. The relatively large error bars on Na and K are due to the fact that (1) Na and K are minor components in the standard and (2) they are more likely to be affected by element loss during beam damage (see below). The use of a liquid-nitrogen cooled specimen holder can reduce the element loss problem, but this technique was not available.

The energy-dispersive spectra can be obtained using either TEM or STEM operational modes. After initial ex-

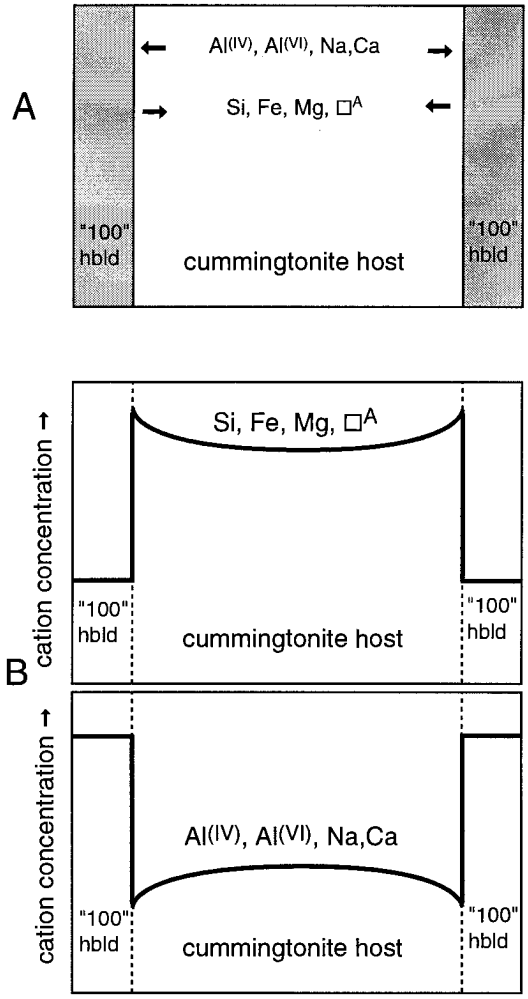

FIGURE 2. (**A**) Schematic drawing of cummingtonite host area between two ''100'' hornblende lamellae. Arrows indicate the diffusing directions of cations and vacancies (□). (**B**) Schematic picture of typically observed cation concentration profiles across the cummingtonite host after stranded diffusion.

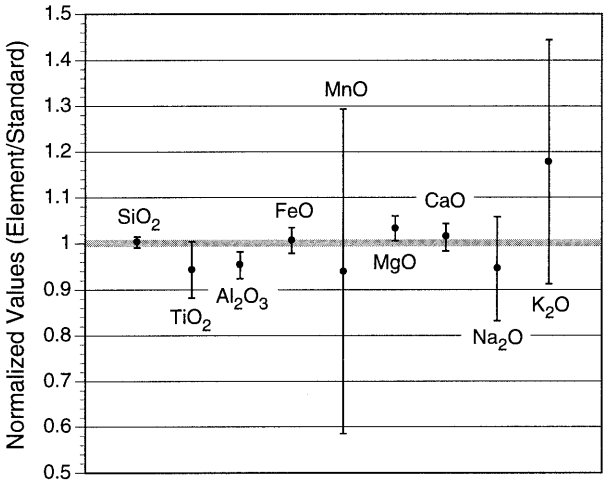

FIGURE 3. Errors of the calibrated k ratios at 200 keV for Philips CM20-FEG electron microscope. For the analyses, a hornblende (Arenai Volcano) from the Smithsonian collection of natural mineral standards for electron microprobe analysis was used (Jarosewich 1975). The errors of k ratios were normalized to 1 (perfect calibration = 1). The error bars represent 1σ errors. The large errors for Mn and K are probably due to the low concentrations of these elements in both the standard and the unknown.

perimentation with analyses in dark-field STEM mode, it was decided that the beam position on the tiny precipitates could be better controlled in the TEM-nanoprobe mode. One problem of EDS analysis in the TEM mode is that features such as nanometer-scale precipitates are not easily visible without diffraction contrast made visible by the use of an objective aperture. However, use of an objective aperture is not possible because it produces X-rays that flood the energy-dispersive detector. We therefore made our energy-dispersive measurements in diffraction mode with the diffraction pattern defocused such that an image of the sample was present in the central beam. The contrast in such an image is essentially the same as in a bright-field image obtained using a small objective aperture, which makes it easier to isolate the small lamellae. The beam is focused onto the tiny lamellae with the second condenser lens while observing the change of magnification within the defocused diffraction pattern. The maximum image magnification seen in the diffraction pattern corresponds to a minimum in beam size.

Radiation-induced sample damage, causing amorphization and loss of alkalis, is a significant problem in analytical TEM (Peacor 1992). The problem of element loss affects more than just the alkali elements and depends on the current density and accelerating voltage of the electron beam, as well as the composition, crystal structure, and temperature of the sample (Champness and Devenish 1990, 1992; Devenish and Champness 1992). In the present study, beam currents were not measured and elemental loss was not investigated in the standards, but beam damage effects were considered. A beam focused to ~1.5 nm diameter caused complete amorphization of the our amphibole samples during a 90 s analysis. To reduce the current density and radiolytic beam damage during our measurements, we used the condenser stigmater to elongate the focused beam parallel to the long axis of $10\bar{1}$ lamellae and thereby increase the irradiated sample volume while maintaining spatial resolution that was high enough to analyze the tiny discs. Using such an astigmatic beam resulted in very little amorphization of our sample during the 90 s analysis time.

Limitations of nanometer-scale microanalysis

Although the transmission electron microscope used in this study is capable of energy-dispersive measurements with an electron beam less than 1 nm in diameter, several factors limit the actual spatial resolution of our measure-

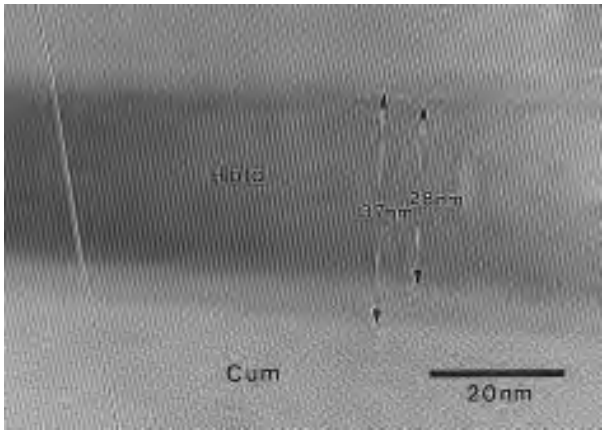

FIGURE 4. An HRTEM image that shows the effect of sample orientation on the spatial resolution. The indistinct border (dark gray rims) of the lamella indicates that it is not perfectly parallel to the electron beam. The variations in the thickness of the gray rims on each side of the hornblende (Hbld) lamella are due to the lenticular shape of the lamella.

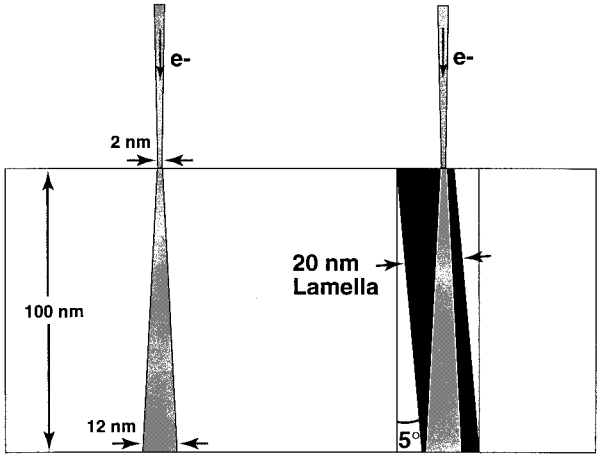

FIGURE 5. A representation of the effect of beam spreading on the resolution for analytical measurements of the nanometer disk-shaped lamella. For a sample thickness of 100 nm and an angle to the electron beam of 5°, the minimum measurable lamella width is about 20 nm.

ments. Although beam spreading is not considered a significant factor in thin-film analysis of micrometer-size features by AEM, beam spreading becomes a limiting factor when attempting to analyze nanometer-scale features. The actual beam spreading that occurs in a sample at a certain acceleration voltage depends on the thickness and density of the thin film sample (Lorimer 1983). Sample thicknesses in the regions we analyzed were not precisely determined, but were estimated to be approximately 100 nm, based upon the separation, as a function of sample tilt, of carbon-contamination spots that form on the top and bottom surfaces of the sample. On the basis of calculated beam broadening of Lorimer (1983) for a Cu sample at 200 kV, as well as for Cu and Al samples at 100 kV, broadening of the electron beam as it passes through 100 nm of amphibole sample should be $\leq$10 nm. Combined with a $\sim$2 nm minimum width of our astigmatic beam perpendicular to the $10\bar{1}$ lamellae, the minimum lamellar width that we could unambiguously measure is $\sim$12 nm. The spatial resolution of our measurements could be improved by decreasing sample thickness to reduce beam broadening, but the X-ray count rate also decreases and the contribution from amorphous surface films and beam damaged material increases.

An additional factor that limits the size of lamellae that we can analyze is the orientation of the lamellae relative to the incident electron beam. In the sample foil that we investigated the $[\bar{1}10]$ zone axis was nearly parallel to the foil normal. HRTEM imaging of the $10\bar{1}$ lamellae along the $[\bar{1}10]$ zone axis (Fig. 4) illustrates the orientation problem. In this image, the coherent hornblende-cummingtonite interfaces that are nearly parallel to $(10\bar{1})$ are diffuse because they are not parallel to the incident beam. In this orientation, the $(10\bar{1})$ plane is inclined by 14.2° from the $[\bar{1}10]$ zone axis used in imaging. This results in an apparent width of 28 nm if one excludes the tilted boundary and 37 nm if one includes it. Because none of the images was obtained with $(10\bar{1})$ exactly parallel to the incident beam, the lamellae widths measured from TEM images are generally greater than the actual widths. Because of the small take-off angle, the sample was tilted by 15° toward the detector so no part of the specimen holder intersects the cone of the X-rays entering the detector. Although fortuitous, this tilting of the sample brought the $10\bar{1}$ lamellae to within approximately 5° of being parallel to the incident beam during energy-dispersive analysis. Although small, the 5° angle between the incident beam and $(10\bar{1})$ results in a substantial increase in the minimum size of lamellae that we could analyze. This orientation effect combined with beam broadening of approximately 10 nm results in a minimum lamellar width limit of approximately 20 nm for our measurements (Fig. 5).

As stated above, beam damage as well as volatilization and diffusion of alkalis in the sample are significant problems in nanometer-scale analyses. During radiolytic beam damage, elemental loss in amphiboles affects each element differently with Na > Ca > Mg > Al > O > Si (Champness and Devenish 1992). The rates of damage and element loss can be determined as a function of current density and other parameters to minimize this effect. In silicates, there is generally a threshold value of electron dose for each element below which no significant element loss occurs (Champness and Devenish 1990, 1992; Devenish and Champness 1992). In the case of tremolite, using 100 kV, the threshold electron current density for Ca loss, is from 4×10^6 A/m^2 to 7×10^7 A/m^2 (Champness and Devenish 1992). The value for 200 kV would be approximately an order of magnitude higher because radiolytic damage decreases with increasing energy. In the present study, current density and its effect on element loss in amphiboles were not determined and

therefore the problem of element loss cannot be evaluated quantitatively. Assuming a beam current value of 0.5 nA (an approximate value from the microscope specifications), the current density within a 1.5 nm diameter beam is $2.8 \times 10^8 A/m^2$, which is an order of magnitude more than the value for Ca loss in tremolite at 100 kV. Assuming a 0.5 nA current and an irradiated area of 2×40 nm, the current density would have been $\sim 6.3 \times 10^6 A/m^2$, which is comparable to the value for Ca loss in amphiboles at 100 kV and approximately an order of magnitude less than the threshold value at 200 kV (Devenish and Champness 1992). It is likely that the current densities that we used were above the threshold value for Na and K loss, but below or comparable to the threshold value for Ca loss. The likely loss of Na makes the degree of edenite substitution involved in exsolution ($Na^A + Al^{+4} \leftrightarrow \square^A + Si^T$) impossible to evaluate accurately. Similarly, if Ca loss were significant, evaluation of the primary substitution ($Ca^{2+} \leftrightarrow Fe^{2+}$) would also be difficult to evaluate. However, if this type of element loss were significant, then the Si contents as well as the Al contents of the damaged lamellae would be high, and this is not the case.

Results

Cummingtonite host

The composition of the cummingtonite (Table 1) was initially determined by EMA, but because of the many nanometer-scale lamellae present in the sample, analysis of the homogeneous host phase was not possible by this method. The only parts of the sample free of nanometer-scale lamellae are the precipitate-free zones that occur adjacent to large hornblende lamellae (Fig. 1), but the 1–2 μm spatial resolution of EMA is not sufficient to resolve fully even these relatively large (0.5–1 μm) regions of precipitate-free cummingtonite.

To examine the cummingtonite composition associated with the final phase of exsolution, we analyzed the host between nanometer-scale lamellae. The average of 50 such AEM measurements of cummingtonite host is shown in Table 1 along with the EMA data. Comparison of AEM and EMA data shows that the Ca, Na, and Al contents of homogeneous host (AEM data), are significantly lower than those of the EMA data. This simply reflects the fact that the nanometer-scale lamellae are too small and too common to be avoided during EMA. The homogeneous host compositions have considerably less Ca and Al than most published analyses of cummingtonite that coexist with hornblende and are similar to analyses of cummingtonite that coexist with orthoamphibole in low-Ca bulk compositions (see Robinson et al. 1982, Fig. 28). This simularity suggests that many of the cummingtonites associated with hornblende either represent equilibrium at higher temperatures than that of the exsolution investigated here or have nanometer-scale precipitates of hornblende that formed at lower temperatures. Our AEM analyses of cummingtonite between the nanometer-scale hornblende precipitates represent a composition that nearly equilibrated with hornblende at ~300 °C during the latest coherent exsolution event.

Table 1. Electron microprobe (EMA) and analytical electron microscopy (AEM) data for cummingtonite host and "100" and "10$\bar{1}$" hornblende lamellae of sample Q-603C

	EMA (cummingtonite host)	AEM		
		Cummingtonite host	"100" Hbld (early generation)	"10$\bar{1}$" Hbld (disk lamella)
SiO_2	52.66	54.79	41.93	40.77
TiO_2	0.10	0.10	1.52	1.62
Al_2O_3	1.27	0.50	15.55	17.08
Cr_2O_3	0.01	0.12	0.16	0.25
FeO	27.47	28.24	20.39	22.33
MnO	0.37	0.33	0.13	0.09
MgO	15.25	15.42	6.68	6.07
CaO	0.88	0.41	11.78	10.30
Na_2O	0.12	0.07	1.51	1.44
K_2O	0.02	0.02	0.34	0.05
Σ	98.15	100.00	100.00	100.00
Si	7.805	7.968	6.212	6.060
Al	0.195	0.032	1.788	1.940
Σ^T	8.000	8.000	8.000	8.000
Al	0.027	0.054	0.927	1.052
Ti	0.011	0.011	0.169	0.181
Cr	0.001	0.014	0.019	0.029
Fe^{3+}	0.106	0.000	0.000	0.000
Mg	3.370	3.343	1.475	1.345
Fe^{2+}	1.485	1.578	2.410	2.393
$\Sigma^{M1\text{-}M3}$	5.000	5.000	5.000	5.000
Fe^{2+}	1.814	1.856	0.116	0.383
Mn	0.046	0.041	0.016	0.011
Ca	0.140	0.064	1.870	1.640
Na	0.000	0.020	0.000	0.000
Σ^{M4}	2.000	1.981	2.002	2.034
Na	0.034	0.000	0.434	0.415
K	0.004	0.004	0.064	0.009
Σ^A	0.038	0.004	0.498	0.424

Notes: Formulae for minimum estimates of ferric Fe content are given (see Robinson et al. 1982). For the EMA analysis, minimum ferric Fe is obtained by assuming a cation sum exclusive Na + K = 15 (15 eNK); whereas for the AEM data, the all-ferrous formulae (ferric Fe = 0) give the minimum values.

Composition of lenticular 10$\bar{1}$ hornblende lamellae and comparison with earlier generation 100 lamellae

The disc-shaped hornblende precipitates that occur between larger lamellae can have either the 10$\bar{1}$ or 100 orientation, but generally have the opposite orientation of the neighboring large lamellae. The precipitates analyzed here with AEM had predominantly the 10$\bar{1}$ orientation and ranged in size from 10–40 nm in width. Variable or low-Ca and low-Al concentrations from lamellae smaller than about 20 nm indicated that such analyses were composite host-plus-lamellae compositions, which were discarded. Because both Al and Ca are expected to be higher in the hornblende lamellae relative to cummingtonite, the effects of mixed analyses would be seen in a plot of Ca vs. Al as data points along a straight mixing line between the hornblende and cummingtonite end-member compositions (Fig. 6). The absence of such data reflects the fact that we discarded mixed analyses during data collection. The 75 hornblende measurements that were not discarded

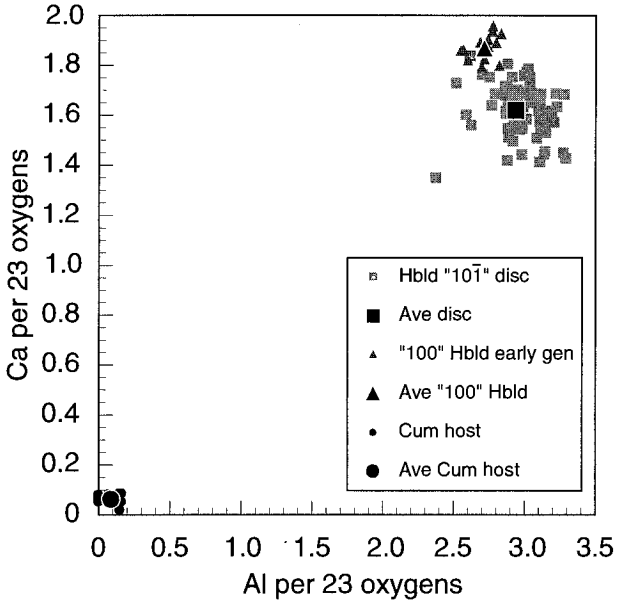

FIGURE 6. A comparison of Ca and Al contents of cummingtonite host with early generation of ''100'' hornblende lamellae and ''101'' disk-shaped, hornblende lamellae. Note the very wide micibility gap.

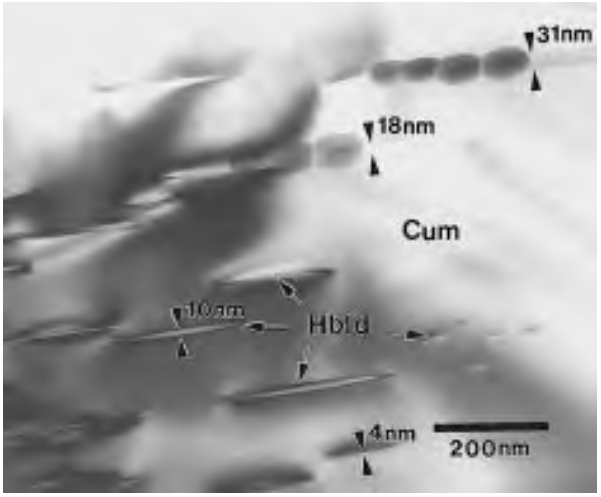

FIGURE 7. A TEM image that shows the traces of the analysis points. An elliptical electron beam was used to obtain better counting statistics and less radiation damage. Image is taken in non-zone axis orientation.

were averaged to obtain the 10$\bar{1}$ hornblende composition shown in Table 1. An example of measured precipitates (Fig. 7) shows contamination spots on hornblende lamellae; note that the spots are elliptical as a result of the astigmatic electron beam used in the measurements. The contamination spots are also larger than the actual beam size used in the analyses. The 10$\bar{1}$ disc data indicate that the late-stage hornblende lamellae are enriched in Al and to a lesser extent in Ca relative to the cummingtonite host. The Ca content is actually less than in the coarse ''100'' hornblende, a surprising result that is discussed below.

Although hornblende is related to cummingtonite by three principal substitution mechanisms, the solvus between the two amphiboles is commonly depicted in terms of Ca content or exchange of Ca^{2+} for Fe^{2+} or Mg^{2+}, with increasing segregation of Ca to hornblende with decreasing temperature (i.e., the solvus widens with respect to Ca at lower T). Surprisingly, this is not found in a comparison of the Ca content of the late-stage 10$\bar{1}$ discs with that of an earlier ''100'' lamella (Table 1, Fig. 6). Klein et al. (1996) showed that the earliest (i.e., highest temperature) generation of 10$\bar{1}$ lamellae exsolved at a temperature around 700 °C, approximately 400 °C above that of this later and lower temperature stage of 10$\bar{1}$ disc-shaped precipitates. The earliest generation 100 lamellae, which also formed at a much higher temperature than the 10$\bar{1}$ disc-shaped precipitates, have a higher Ca content (1.870 vs. 1.640 Ca pfu for the 10$\bar{1}$ discs). This is inconsistent with Ca concentrations expected from the relative temperatures of exsolution.

The exsolution of hornblende from cummingtonite is more complex than simply Ca-Fe or Ca-Mg exchange and can also be described in terms of the edenite or tschermakite substitutions by looking at Al or Na content vs. temperature. The anomalously low Ca contents in the 10$\bar{1}$ discs are not paralleled by the Al contents. The 10$\bar{1}$ discs have considerably more Al than the earliest generation 100 lamellae (2.992 vs. 2.715 Al pfu), as expected because the edenite and tschermakite substitutions involve Al exchange and the cummingtonite-hornblende solvus also widens with respect to Al. Looking at the Na content, we see that the tiny 10$\bar{1}$ discs also have less Na than the larger 100 lamellae. This suggests that, although the compositions of the 10$\bar{1}$ discs are probably metastable, the effectiveness of the various substitution mechanisms may be different at low temperature. An alternative explanation is that the Ca, like the Na, is preferentially lost during the analyses. These interpretations are discussed further below.

Cummingtonite host profiles

Compositional profiles between lamellar systems show the extent of equilibration between the host and lamellae and document the chemical zonation within the host phase. One profile was obtained along a 525 nm line between two 10$\bar{1}$ discs with an average spacing of 33 nm between analysis spots (Fig. 8A). A second profile was measured along a 675 nm line between an earlier generation 100 lamella and an area of late-stage 10$\bar{1}$ discs with an average spacing of 62 nm (Fig. 8B).

The results of the profile measurements are shown in Figure 9. Although the data in the profiles have significant scatter, they are useful for showing the general zoning patterns of Al, Si, Ca, and Mg within the host cummingtonite. Na profiles are not shown because of the large scatter in the data as a result of Na loss during analysis. In the case of Al, both profiles (Fig. 9A and 9B)

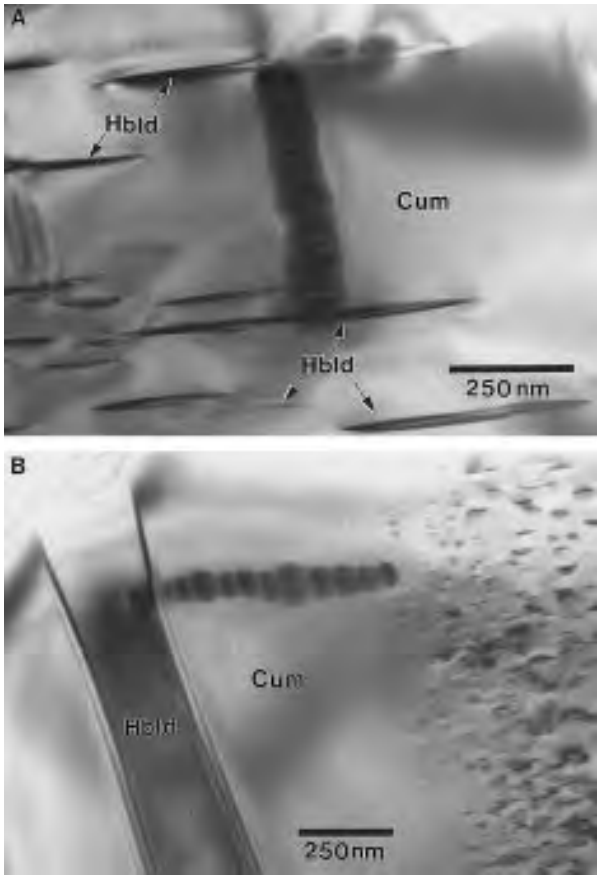

FIGURE 8. TEM images that show the locations of two analytical profiles in the cummingtonite (Cum) host between: (**A**) two ''10$\bar{1}$'' disk-shaped lamellae and (**B**) a large ''100'' hornblende (Hbld) lamella and the area that contains the ''10$\bar{1}$'' disc-shaped, hornblende lamellae. Images are taken in non-zone axis orientations.

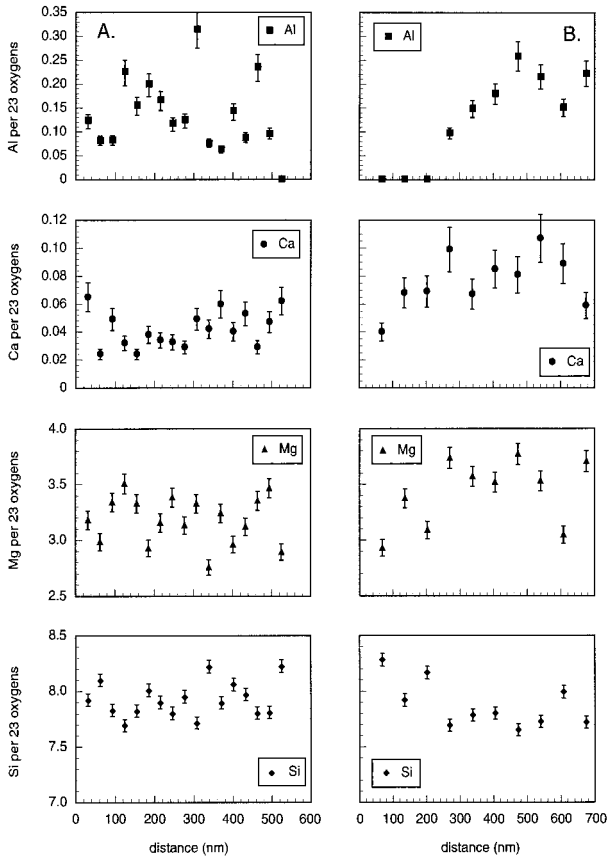

FIGURE 9. Plots of distance vs. concentration of Si, Al, Ca, and Mg in the cummingtonite host between: (**A**) two disc-shaped lamellae and (**B**) a large ''100'' hornblende lamella and the area that contains the disc-shaped, hornblende lamellae (see also Fig. 8).

show a slight downward concavity with higher Al contents about mid-way between the hornblende. This is consistent with depletion of Al by diffusion in regions directly adjacent to the lamellae, but with insufficient time for complete equilibration of the host with the lamellae. Similarly, the Si profiles show slight upward concavity, indicative of Si diffusion away from the growing hornblende lamellae, but with insufficient time for complete equilibration across the distance between lamellae. In the case of Si diffusion between 10$\bar{1}$ lamellae (Fig. 9A), the upward concavity is subtle and may indicate near equilibration of Si content. Interpretation of the Mg profiles is even less clear. Between the 10$\bar{1}$ and 10$\bar{1}$ lamellae, the Mg profile appears to be slightly concave downward as expected from diffusion of Mg out of the growing hornblende. However, between the two 10$\bar{1}$ lamellae, Mg appears to be flat or slightly concave upward, which is not consistent with diffusion of Mg out of the hornblende.

The Ca profile between the 100 and 10$\bar{1}$ lamellae is concave downward as expected, but, like Mg, it is horizontal or slightly concave upward between the two 10$\bar{1}$ lamellae. The nearly flat profiles of Ca and Mg between 10$\bar{1}$ lamellae suggests that diffusion of these elements was not the rate-limiting factor in the hornblende exsolution. If slow diffusion of M4 cations was the rate-limiting step for exsolution at 300 °C, we should see downward concavity in the Ca and Mg profiles between 10$\bar{1}$ lamellae. A possible interpretation of this observation is discussed below.

The average Ca content in the profile between 10$\bar{1}$ discs (Fig. 9A) is actually lower than in the profile between the early 100 lamellae and the area rich in 10$\bar{1}$ precipitates (Fig. 9B), which suggests that the growth of 10$\bar{1}$ discs more effectively depletes the cummingtonite host of Ca than diffusion to the growing 100 lamellae. This may result from diffusion to additional 10$\bar{1}$ discs that were nearby but out of the plane of the thin foil and therefore not seen in TEM. Figure 10 shows a schematic distribution of Ca content over an area that includes the host phase, coarse lamella, and the disk lamellae on the basis of the AEM results.

The most striking difference between the 100-10$\bar{1}$ and 10$\bar{1}$-10$\bar{1}$ profiles is in the Al and Ca concentrations, as

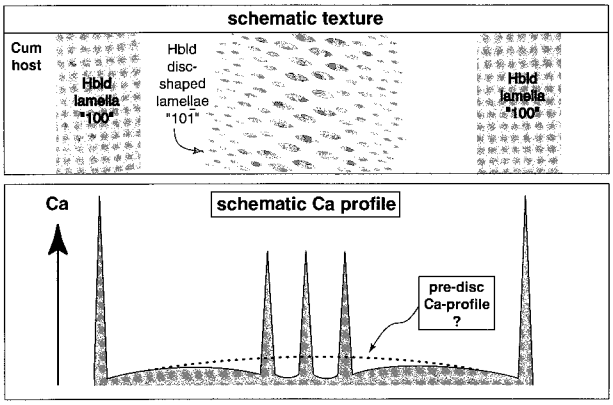

FIGURE 10. Schematic distribution of the Ca content in the cummingtonite host and the two hornblende lamellae systems on the basis of the AEM data.

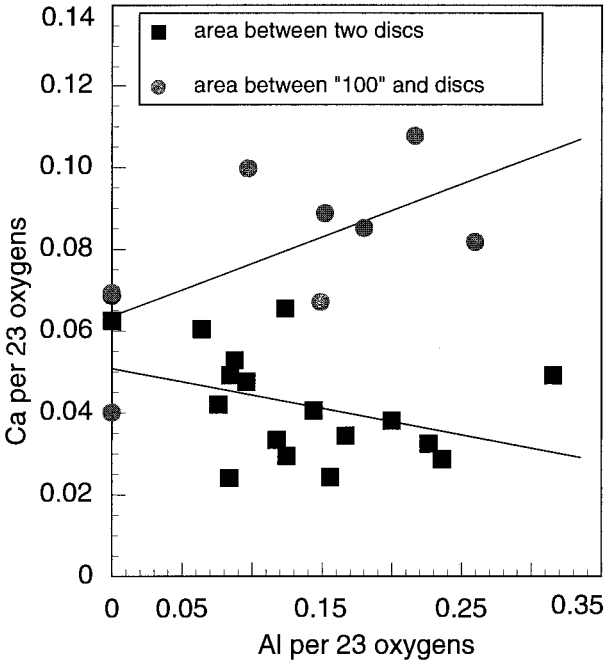

FIGURE 11. Plot of Ca vs. Al for the analytical profiles of the host cummingtonite in Figure 8. For cummingtonite between two disc-shaped hornblende lamellae (see Fig. 8A) the Ca and Al contents show a negative correlation and (Fig. 8B) between larger ''100'' hornblende lamella and area of disc-shaped hornblende lamellae (see Fig. 8B) shows positive correlation.

illustrated in a plot of Ca vs. Al (Fig. 11). Because both Al and Ca were diffusing into growing hornblende precipitates during the final stages of exsolution, we expect the Ca and Al contents from the host profile measurements to have positive correlations in the regions of new hornblende growth. This is exactly what we see in the data from the 100-10$\bar{1}$ profiles (Fig 8B and 9B), where the final phase of hornblende formation occurred at two different locations: (1) through growth at the pre-existing 100 hornblende lamella and (2) through nucleation and growth of 10$\bar{1}$ discs. In contrast, the data from the 10$\bar{1}$-10$\bar{1}$ profiles show a weak negative correlation between Ca and Al. This suggests that the processes that controlled the distribution of these elements within the region of nucleation and growth of 10$\bar{1}$ discs were different than in the region of 100 lamellae growth. The fact that the Ca contents are lower in the 10$\bar{1}$-10$\bar{1}$ profiles suggests that the edenite or tschermakite substitutions were less active than the Ca-Fe^{2+} exchange during disc precipitation than they were when most of the precipitate-free zone formed.

DISCUSSION

Observations

The surprising observation that the late-stage 10$\bar{1}$ lamellae have less Ca and more Al than the earlier generation 100 lamellae suggests that an analytical artifact may be involved. One potential explanation for the low Ca contents of the 10$\bar{1}$ lamellae is that the data represent mixed hornblende-cummingtonite analyses. We can rule out this artifact because we see no evidence for mixing in the Al vs. Ca plot of Figure 6, and such a mixed analysis between hornblende and cummingtonite could not explain the higher Al content in the disc lamellae. Another potential artifact could arise from our k factors. This is unlikely because we used a hornblende standard with sufficient concentrations of Ca and Al for precision of approximately $\pm 3\%$.

Another potential problem with the 10$\bar{1}$ measurements is the loss of Ca as a result of radiolytic beam damage. As discussed above, the rate of elemental loss depends on the element as well as on the sample and microscope parameters. It is possible that the current densities used in the measurements of the 10$\bar{1}$ hornblende discs were above the threshold values for loss of Na, K, Ca, and Mg, but below the threshold values for Fe, Al, and other elements. Although this could explain the low values of Ca and Mg relative to Al and Fe, it cannot explain the low Si contents of the 10$\bar{1}$ hornblende discs. The low Si is not consistent with elemental loss because Si is the one element not lost in beam damage of silicates. In fact, after extreme radiolytic beam damage, the residual material from many silicate minerals, including amphiboles, is SiO_2 (Champness and Devenish 1992; Devenish and Champness 1992). Although Ca loss during measurement of the 10$\bar{1}$ hornblende discs cannot be ruled out completely, it cannot fully account for the tschermakitic compositions of these precipitates.

The high Al content with corresponding low Ca content in the discs is surprising, and according to Leake (1978) the 10$\bar{1}$ discs are ferro-tschermakite rather than ferro-hornblende. The high Al contents do not appear to be purely the result of the edenite-like substitution, because the A site is only partially occupied. Because Na and K were partially lost during our analyses, it is impossible to determine the extent of the edenite substitution. The combination of high Al in tetrahedral coordi-

nation and relatively low Mg in octahedral coordination indicates that the tschermakite-like substitution was important in the exsolution of both $10\bar{1}$ discs and 100 lamellae.

A possible explanation for the low Ca and high Al contents of the $10\bar{1}$ discs is that the cummingtonite between the larger 100 lamellae had excess Al relative to Ca before the precipitation of the $10\bar{1}$ discs. As exsolution proceeded and the $10\bar{1}$ discs nucleated, both Ca and Al were rejected from the cummingtonite and driven into the growing hornblende precipitates resulting in normal hornblende compositions. During growth of the $10\bar{1}$ discs, the Ca content of the host cummingtonite was depleted leaving excess Al. As the cummingtonite structure continued to reject Al, the growing $10\bar{1}$ discs became increasingly more tschermakitic in composition. This interpretation implies that the tschermakitic $10\bar{1}$ hornblende discs may be close to the equilibrium composition coexisting with an Al-rich cummingtonite. This interpretation is consistent with the very low Ca contents of the host cummingtonite, but it does not explain the weak negative correlation between Ca and Al in the $10\bar{1}$-$10\bar{1}$ profile data (Fig. 11). The downward concavity of the Al profile between $10\bar{1}$ discs suggests that Al is the slowest diffusing species in the cummingtonite and that the extent of Al segregation was diffusion controlled.

Development of the composition profiles

The observed compositional profiles represent the final arrested state of the cummingtonite host trying to reach an equilibrium composition. The concave compositional profiles for Al and Ca (Fig. 9) may have formed as a result of further growth of the 100 hornblende lamellae because these preexisting hornblendes do not require nucleation. Upon further cooling, nucleation and growth of the $10\bar{1}$ hornblende lamellae occurred between the coarser 100 hornblende lamellae where the highest concentrations of Ca and Al remained. The average size of the lenticular precipitates decreases away from the center of the zone of precipitation. Assuming a random distribution of homogeneous nucleation sites, the size distribution and nucleation rate were probably related to the actual amounts of Ca and Al available within different regions of the concentration profiles.

Following the formation of disc-shaped $10\bar{1}$ hornblende lamellae, the factors that controlled the concentration gradients within the zone of precipitation appear to have changed somewhat. The downward concavity of the Al profile between $10\bar{1}$ discs suggests that Al is the slowest diffusing species in the cummingtonite and that the extent of Al segregation during growth of the $10\bar{1}$ discs was diffusion controlled. The weak upward concavity in the Ca profile between $10\bar{1}$ discs must have developed by a different process because normal diffusion control during growth produces downward concavity of Ca whereas equilibration produces a flat Ca profile.

The Gibbs-Thomson (capillary) effect (e.g., Porter and Easterling 1992) could explain upwardly concave Ca profiles through differences in the radius of curvature of the particles. All deviations from a perfect single crystal (e.g., surfaces, grain boundaries, interphase interfaces, dislocations, and so forth) cause an increase of the free energy of the observed system. The interfacial energy term increases at constant T with the curvature of the interface between precipitate and host, therefore the free energy increases with increasing interface curvature. This increase, known as the capillarity or the Gibbs-Thomson effect, is very sensitive to the size of the precipitates and can produce large differences in solubility for nanometer-scale precipitates, with the effect increasing with the decreasing size of the precipitates. During coarsening, the larger (growing) precipitates have progressively decreasing interfacial curvature of their interfaces and therefore lower surface energies per unit volume and lower total free energies relative to the smaller dissolving (shrinking) discs. Variation in precipitate size and interfacial curvature provides the driving force for coarsening. An important consequence of the Gibbs-Thomson effect is that the concentrations of hornblende components increase in the adjacent cummingtonite near $10\bar{1}$ discs that have a high radius of curvature. This effect is illustrated on a schematic G-X curve (Fig. 12A) (see also Porter and Easterling 1992).

In a system of newly formed nano-precipitates in which the coarsening process had just begun, growing and shrinking discs would be distributed throughout the zone of precipitates (e.g., Fig. 12B). As a result, element concentration profiles between pairs of lamellae could take various appearances, which would be strongly influenced by the types of the lamellae pairs (growing-growing, shrinking-shrinking, or growing-shrinking). For example, a Ca profile between shrinking and growing lamellae would show increasing Ca away from the growing lamella as the shrinking lamella is approached (Fig. 12B and 12C, profile A-A′); a Ca profile between two shrinking lamellae would decrease away from both lamellae if there is a growing lamellae in the area (Fig. 12B and 12C, profile B-B′). The profile B-B′ corresponds to the measured Ca profile of the cummingtonite between two disc-shaped precipitates (Fig. 8A). It is noteworthy that the Al profiles are not the same as the Ca profiles, suggesting that little Al diffusion occurred during coarsening.

The importance of the Gibbs-Thomson effect decreases as size (radius of curvature) of the precipitates increase. Assuming spherical particles, the differences in free energy because of the Gibbs-Thomson effect for radii from 1 to 100 nm can be significant (Porter and Easterling 1992). The disc-shaped, nano-lamellae in this study are seen only in two dimensions and average about 4×600 nm in size. Assuming that the third dimension lies between 50 and 600 nm, the effective radius [cube root of $4 \times 600 \times$ (50 or 600)] is about 49–113 nm, suggesting that the Gibbs-Thomson effect could be an important factor. The Gibbs-Thomson dissolution and growth scenario described above, if correct, must represent the final state frozen into the system during this complex exsolution history.

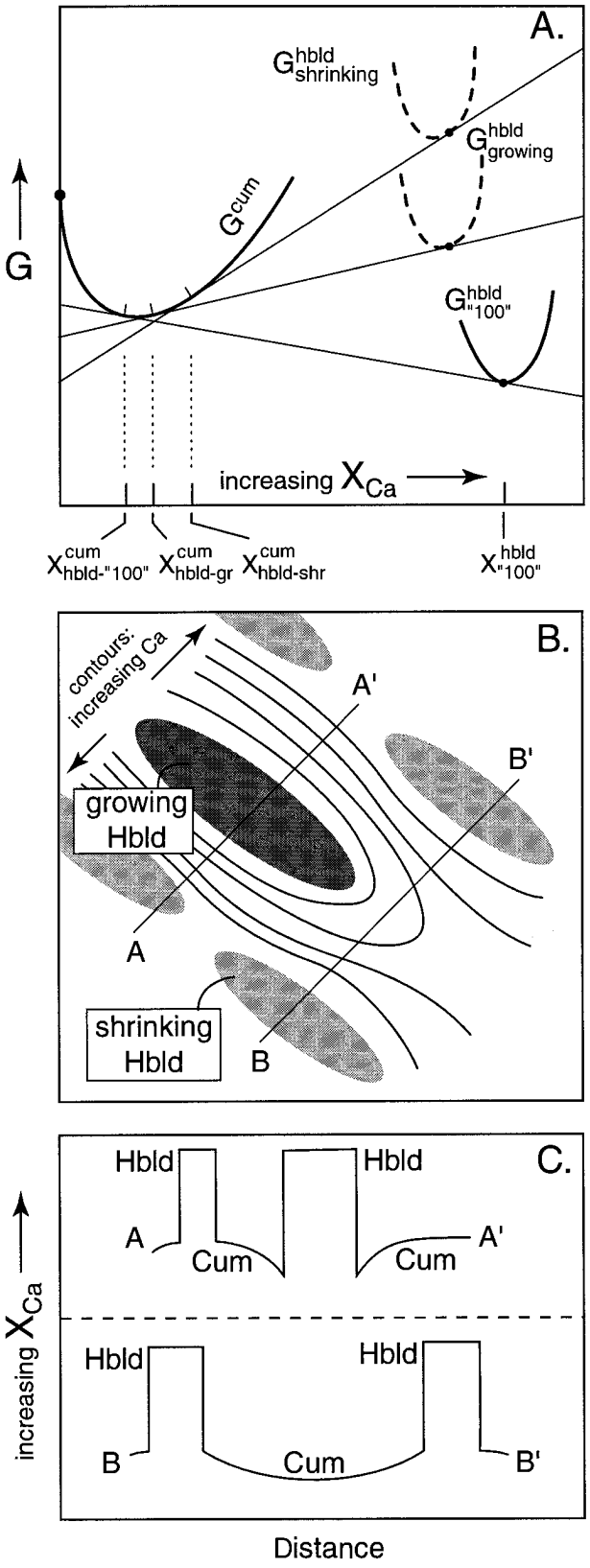

FIGURE 12. A possible explanation for the Ca concentration in the cummingtonite (Cum) host. (**A**) Schematic *G-X* curves for the cummingtonite host and various hornblende (Hbld) lamellae. (**B**) Schematic isopleths for Ca content between shrinking and a postulated lenticular hornblende lamellae that is growing. Note that profile A-A′ cuts a growing and a shrinking lamella, while profile B-B′ cuts two shrinking lamellae. (**C**) Schematic Ca contents for the profiles given in part B.
←

CONCLUSIONS

Because the spatial resolution of the electron microprobe is restricted to a diameter of about 1.5 μm, it is not possible to quantify the chemical composition of submicrometer scale hornblende lamellae or the cummingtonite between lamellae by EMA. For samples with complex exsolution microstructures like multiply-exsolved cummingtonite from New England, analytical TEM is essential for determining the compositions of lamellae and host. However, limitations of the AEM technique from low counting statistics, beam damage, and absorption must be carefully taken into account. By using a field-emission instrument, hornblende precipitates as small as a few nanometers may be quantitatively analyzed. However, because of beam broadening effects and precipitate orientations we were only able to analyze quantitatively precipitates as small as 20 nm. Radiolytic beam damage can also limit the resolution of the measurement if the current density in the probe is above the thresholds for loss of various elements.

Compositions of the nanometer-scale hornblende discs from the youngest stage of exsolution indicate much lower Ca contents than in the coarser and higher *T* lamellae. Although it is possible that some of this effect may be due to Ca loss during our analyses, differential elemental loss cannot account for the tschermakite-rich compositions of the nanometerscale hornblende precipitates. The late-stage discs appear to represent tschermakitic amphibole trying to equilibrate with an Al-rich cummingtonite depleted in Ca by the growth of earlier hornblende lamellae. The compositional zoning of the host with respect to several elements favors the interpretation that the disc-shaped precipitates represent a metastable and arrested stage of exsolution. Composition profiles between the disc-shaped precipitates suggest the rate of Ca diffusion in cummingtonite is faster than that of Al. This is certainly related to the coupled nature of Al substitutions in the amphibole structure vs. the homovalent exchange of Ca for Fe^{2+} or Mg between cummingtonite and hornblende. Additionally, the concavity of Ca vs. Al compositional profiles between the nano-lamellae seem to indicate that the exsolution process stopped during a coarsening phase of lamellae development.

ACKNOWLEDGMENTS

This work was supported by the Deutsche Forschungsgemeinschaft (DFG) grant number Cz 19/4-2 to M. Czank and J.C. Schumacher. Special

thanks go to Kurt Hollocher for supplying the sample Q-603C and to David Veblen, Peter Robinson, and Michael Czank whose ongoing interest in "amphibology" have provided insight and inspiration. Pamela Champness and Gene Smelik greatly improved this work with critical and very constructive reviews.

REFERENCES CITED

Bollman, W. and Nissen, H.-U. (1968) A study of optimal phase boundaries: The case of exsolved feldspars. Acta Crystallographica, A24, 546–557.

Cahn, J.W. (1968) Spinodal decomposition. Transactions of the Metallurgical Society of AIME, 242, 166–180.

Champness, P. and Devenish, R. (1990) Elemental mass loss in silicate minerals during X-ray analysis. Transaction of the Royal Microscopic Society, 1, 177–180.

——— (1992) Radiation damage in silicate minerals: implications for AEM. Electron Microscopy, Vol. 2, EUREM 92, 541–545.

Cliff, G. and Lorimer, G.W. (1975) The quantitative analysis of thin specimens. Journal de Microscopie, 103, 203–207.

Czank, M., Klein, U., Mayer, J., and Schumacher, J.C. (1993) Anwendung der elektronenmikroskopischen Abbildung (ESI) zum Nachweis von Entmischungen im Nanometermassstab. Beihefte zum European Journal of Mineralogy, 5, 149.

Czank, M., Mayer, J., and Klein, U. (1997) Electron spectroscopic imaging (ESI): A new method to reveal the existence of nm-scaled exsolution lamellae. European Journal of Mineralogy, in press.

Devenish, R. and Champness, P. (1992) The rate of mass loss in silicate minerals during X-ray analysis. Proceedings of the 13th International Congress on X-ray Optics and Microanalysis, Institute of Physics, London, 233–236.

Fleet, M.E. (1982) Orientation of phase and domain boundaries in crystalline solids. American Mineralogist, 67, 926–936.

——— (1984) Orientation of feldspar intergrowths: Application of the lattice misfit theory to cryptoperthites and *e*-plagioclase. Bulletin de Minéralogie, 107, 509–519.

——— (1985) Orientation of phase and domain boundaries in crystalline solids: reply. American Mineralogist, 70, 130–133.

Fleet, M.E. and Arima, M. (1985) Oriented hematite inclusions in silimanite. American Mineralogist, 70, 1232–1237.

Fleet, M.E., Bilcox, G.A., and Barnett, R.L.(1980) Oriented magnetite inclusions in pyroxenes from the Greenville Province. Canadian Mineralogist, 18, 89–99.

Ganguly, J., Chakraborty, S., Sharp, T.G., and Rumble, D. III (1996) Constraints on the time scale of biotite grade metamorphism during the Acadian Orogeny from a natural garnet-garnet diffusion couple. American Mineralogist, 81, 1208–1216.

Hollocher, K.T. (1985) Geochemistry of metamorphosed volcanic rocks in the Middle Ordovician Partridge Formation, and amphibole dehydration reactions in the high-grade metamorphic zones of central Massachusetts, 275 p. Contribution No. 56, Ph.D. thesis, Department of Geology and Geography, University of Massachusetts, Amherst.

——— (1993) Geochemistry and origin of volcanics in the Ordovician Partridge Formation, Bronson Hill anticlinorium, west-central Massachusetts. American Journal of Science, 293, 671–721.

Jaffe, H.W., Robinson, P., and Klein, C. (1968) Exsolution lamellae and optic orientation of clinoamphiboles. Science, 160, 776–778.

Jarosewich, E. (1975) Chemical analysis of two microprobe standards. Smithsonian Contributions to the Earth Sciences, 14, 85–86.

Klein, U., Schumacher, J.C., and Czank, M. (1996) Mutual exsolution in hornblende and cummingtonite: Compositions, lamellar orientations, and exsolution temperatures. American Mineralogist, 81, 928–939.

Leake, B.E. (1978) Nomenclature of amphiboles. Canadian Mineralogist, 16, 501–520.

Lorimer, G.W. (1983) Quantitative X-ray microanalysis of thin specimens. In J.N. Chapman and A.J. Craven, Eds., Quantitative electron microscopy, p. 305–339. Proceedings of the Twenty-Fifth Scottish Summer School in Physics.

Lorimer, G.W. and Champness, P.E. (1973) Combined electron microscopy and analysis of an orthopyroxene. American Mineralogist, 58, 243–248.

Lorimer, G.W., Nasir, M.J., Nicholson, R.B., Nuttall, K., Ward, D.E., and Webb, J.R. (1972) The use of an analytical electron microscope (EMMA-4) to investigate solute concentrations in thin metal foils. In G. Thomas, Ed., Electron microscopy and structure of materials, p. 222–234. University of California Press, Berkeley.

Lorimer, G.W., Razik, N.A., and Cliff, G. (1973) The use of the analytical electron microscope EMMA-4 to study the solute distribution in thin foils: some applications to metals and minerals. Journal de Microscopie, 99, 153–164.

Meissner, E., Sharp, T.G., and Chakraborty, S. (1996) Analytical TEM measurement (ATEM) of sub-μm diffusion profiles. Terra Nova 8, Abstract supplement 1, 44.

Peacor, D.R. (1992) Analytical electron microscopy: X-ray analysis. In Mineralogical Society of America Reviews in Mineralogy, 27, 113–140.

Porter, D.A. and Easterling, K.E. (1992) Phase transformation in metals and alloys, 514 p. Van Nostrand Reinhold Ltd., New York.

Robin, P.-Y.F. (1974) Stress and strain in crypthoperthite lamellae and the coherent solvus of alkali feldspars. American Mineralogist, 59, 1299–1318.

——— (1977) Angular relationships between host and exsolution lamellae and the use of the Mohr circle. American Mineralogist, 62, 127–131.

Robinson, P., Jaffe, H.W., Klein, C., and Ross, M. (1969) Equilibrium coexistence of three amphiboles. Contributions to Mineralogy and Petrology, 22, 248–258.

Robinson, P., Jaffe, H.W., Ross, M., and Klein, C. (1971) Orientations of exsolution lamellae in clinopyroxenes and clinoamphiboles: Consideration of optimal phase boundaries. American Mineralogist 56, 909–939.

Robinson, P., Ross, M., Nord, G.L., Jr., Smyth, J.S., and Jaffe, H.W. (1977) Exsolution lamellae in augite and pigeonite: fossil indicators of lattice parameter at high temperatures and pressures. American Mineralogist, 62, 857–873.

Robinson, P., Spear, F.S., Schumacher, J.C., Laird, J., Klein, C., Evans, B.W., and Doolan, B.L. (1982) Phase relations of metamorphic amphiboles: natural occurrence and theory. In Mineralogical Society of America Reviews in Mineralogy, 9B, 1–211.

Ross, M. Papike, J.J., and Weiblen, P.W. (1968) Exsolution in clinoamphiboles. Science, 159, 1099–1104.

Ross, M., Papike, J.J., and Shaw, K.W. (1969) Exsolution textures in amphiboles as indicators of subsolidus thermal histories. Mineralogical Society of America Special Paper 2, 275–299.

Schumacher, J.C. (1988) Stratigraphy and geochemistry of the Ammonoosuc Volcanics, central Massachusetts and southwestern New Hampshire. American Journal of Science, 288, 619–663.

Schumacher, J.C., Klein, U., and Czank, M. (1993) Temperatures of mutual exsolution in hornblende and cummingtonite as possible evidence for varying regional metamorphic cooling rates. Geological Society of America Abstracts with Programs 25, A101.

Smelik, E.A. and Veblen, D.R. (1989) A five amphibole assemblage from blueschits in northern Vermont. American Mineralogist, 74, 960–965.

——— (1991) Exsolution of cummingtonite from glaucophane: A new orientation for exsolution lamellae in clinoamphiboles. American Mineralogist, 76, 971–984.

——— (1993) A transmission and analytical electron microscope study of exsolution microstructures and mechanisms in the orthoamphiboles anthophyllite and gedrite. American Mineralogist, 78, 511–532.

Smelik, E.A., Nyman, M.W., and Veblen, D.R. (1991) Pervasive exsolution within the calcic amphibole series: TEM evidence for a miscibility gap between actinolite and hornblende in natural samples. American Mineralogist, 76, 1184–1204.

Vernon, R.H. (1962) Coexisting cummingtonite and hornblende in amphiboles from Duchess, Queensland, Australia. American Mineralogist, 47, 360–370.

Willaime, C. and Brown, W.L. (1974) A coherent elastic model for the determination of the orientation exsolution boundaries: Application to the feldspars. Acta Crystallographica, 8, 301–308.

——— (1985) Orientation of phase and domain boundaries in crystalline solids: discussion. American Mineralogist, 70, 124–129.

MANUSCRIPT RECEIVED NOVEMBER 25, 1996
MANUSCRIPT ACCEPTED JULY 28, 1997